J. Fluid Mech. (1975), *vol.* 72, *part* 1, *pp.* 145–160
Printed in Great Britain

Instability of flow in a curved alluvial channel

By FRANK ENGELUND

Institute of Hydrodynamics and Hydraulic Engineering,
Technical University of Denmark, Lyngby

(Received 7 February 1975)

This paper deals with two main problems concerning flow in curved alluvial channels. First, the large-scale bottom geometry that develops through the interaction of flow and sediment motion is determined. Second, experiments in an annular flume indicate that the bed is unstable and that this particular instability leads to the formation of a certain number of scour holes. This is explained by a linear stability analysis.

1. Introduction

A characteristic feature of the mechanics of alluvial channels is that the bed is self-formed by the interaction of flow and sediment motion. The large amount of theoretical and experimental work on flow in straight channels has been summarized in several books, such as those of Raudkivi (1967), Graf (1971) and Larras (1972). The flow in curved channels, river bends or meanders has attracted considerably less attention. In the case of prescribed bottom geometry, the flow may be described by methods summarized by Rozovskii (1961). The influence of channel curvature on flow resistance and the sediment transport rate has been investigated experimentally by Zimmermann & Kennedy (1973), while the development of bottom geometry has been studied by Hooke (1974). In a recent dissertation, Zimmermann (1974) has discussed the flow and bed instability in a channel bend and arrived at results in some respects similar to those presented below, but using a different approach. Apart from this, little work has been done in this field from the theoretical side despite the fact that, in practice, curved and meandering streams are more common than straight ones.

In the investigation described in this paper, the aim was to create a flow with the simplest possible boundary conditions. The experiments were carried out in a closed annular flume with rectangular cross-section; see figure 5. The bottom was covered with a coarse granular material consisting of uniform 3 mm plastic particles with a specific gravity of 1·4 g/cm^3. The flow was brought about by rotation of the cover and was consequently of the Couette type, but for two reasons considerably more complicated than plane Couette flow: (i) as the flow took place in a curved channel, it became helical and (ii) the bed was not plane and horizontal but approached some surface of revolution, depending on the interaction of the flow and sediment motion.

As will be demonstrated, there was a third and more complex difficulty, viz. that such a bed is usually unstable and breaks up, forming a certain (integer)

number of undulations. As long as the amplitude of these sand waves is small, it grows exponentially with time and the perturbation is very regular and sinusoidal. As the amplitude becomes larger, the whole pattern becomes irregular and approaches a pseudo-steady situation where the sand waves exhibit many of the stochastic features characteristic of ripples and dunes in straight channels. There are, however, some very obvious differences between the sand-wave formation in a curved flume and that in a straight flume. First, it is remarkable that, for a curved flume, in the early stages of development the sand waves are very nearly sinusoidal (in the flow direction), while dunes and ripples are almost triangular in shape right from the beginning. The mature sand waves in a curved flume have the character of migrating scour holes, as described by Zimmermann (1974), but the steep slope is not always found on the lee side of the wave as it is in straight channels.

The theoretical analysis is carried out in two steps: the calculation of the basic flow (when the sand bottom is a surface of revolution) and the stability analysis, which predicts whether or not a certain regular perturbation will increase or decrease. In the following analysis, it is assumed that the channel depth is small compared with its width.

2. The three-dimensional Couette flow

Steady and uniform flow in channel bends may be calculated by the methods presented in the monograph by Rozovskii (1961). One of the basic problems in three-dimensional flow of this type is that the distribution of the centrifugal force over a vertical cross-section is non-uniform and hence cannot be adequately balanced by the uniformly distributed pressure gradient, with the result that the flow becomes helical.

The flow is most conveniently described in polar co-ordinates, as indicated in figure 1. If the radius of curvature is large compared with the depth and the depth variation is moderate, the flow equations may be written in the form

$$\tau_0/\rho = \epsilon \partial v_\theta/\partial z, \tag{1}$$

$$-\frac{v_\theta^2}{r} = -\frac{\partial}{\partial r}(gh) + \frac{\partial}{\partial z}\left(\epsilon \frac{\partial v_r}{\partial z}\right) = -g\frac{\partial h}{\partial r} + \frac{\partial}{\partial z}\left(\frac{\tau_r}{\rho}\right), \tag{2}$$

where τ_0 is the bed shear stress, ρ the fluid density, ϵ the eddy viscosity, g the acceleration due to gravity and h the piezometric level. Equation (1) expresses the fact that the shear stress τ_0 is transferred from the moving upper plate to the bottom of the channel without a change in magnitude. Equation (2) expresses the fact that the difference between the centrifugal and the pressure forces is balanced by means of the radial shear-stress component τ_r.

Before the equations can be solved, it is necessary to specify the value of the eddy viscosity ϵ. The most natural procedure is to adapt the expression suggested by Reichardt (1959) to ordinary turbulent Couette flow:

$$\epsilon = 0{\cdot}4U_f z(1-z/y), \tag{3}$$

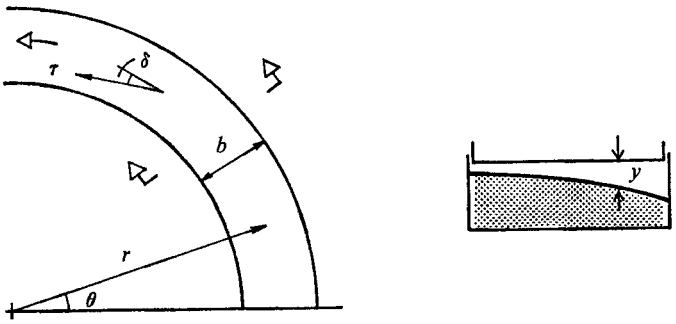

(*a*) (*b*)

FIGURE 1. Definition sketch. (*a*) Plan view and (*b*) cross-section.

where 0·4 is the Kármán universal constant and y is the local depth, as indicated in figure 1. U_f is the friction velocity, defined as

$$U_f = (\tau_0/\rho)^{\frac{1}{2}}. \tag{4}$$

After insertion of (3) and (4), (1) is easily integrated:

$$\frac{v_\theta}{U_f} = 2{\cdot}5 \ln \frac{\zeta}{1-\zeta} + C, \tag{5}$$

where $\zeta = z/y$ and C is a constant that must be determined from the boundary condition at the bed. Because of the large sediment size, this condition is that the distribution near the bed must approach the general velocity distribution for turbulent flow in hydraulically rough pipes. As (5) gives a logarithmic distribution, the condition will be satisfied if it is required that the velocity vanishes at a height $\frac{1}{30}k_b$ above the theoretical bed level, where k_b is the equivalent sand roughness of the bed. This gives the equation

$$\frac{v_\theta}{U_f} = 2{\cdot}5 \ln \frac{\zeta}{1-\zeta} + 2{\cdot}5 \ln \frac{30y}{k_b}. \tag{6}$$

The upper plate is assumed to rotate with angular speed Ω. An expression for its velocity is obtained if we take $z = y - \frac{1}{30}k_t$, where k_t is the roughness of the plate:

$$\frac{\Omega r}{U_f} = 2{\cdot}5 \left[\ln \frac{30y}{k_t} + \ln \frac{30y}{k_b} \right].$$

In fact, the upper plate was not rough, and hence the first term in the brackets must be replaced by the expression for smooth walls:

$$\frac{\Omega r}{U_f} = 2{\cdot}5 \left[\ln \frac{9U_f y}{\nu} + \ln \frac{30y}{k_b} \right], \tag{7}$$

where ν is the kinematic viscosity of the water. Equation (7) may be used to calculate the shear stress exerted by the upper plate for a given angular speed, provided that k_b is known. In the present case, k_b was estimated to be about 6 mm, but since a logarithm is a slowly varying function, the result is not sensitive to errors in this estimate.

Knowing the distribution (6) of v_θ it is now possible to perform an integration of (2) and thus determine the magnitude and distribution of the radial velocity component v_r. Substituting $v_\theta = U_f f(\zeta)$ and integrating once leads to

$$\frac{\tau_r}{\rho y} = -\frac{U_f^2}{r}\int_0^\zeta f^2(\xi)\,d\xi + \zeta g\frac{\partial h}{\partial r} + C, \tag{8}$$

where C is a constant of integration to be determined later. Now, introducing the expression

$$\frac{\tau_r}{\rho} = \kappa U_f \zeta(1-\zeta)\frac{\partial v_r}{\partial \zeta}$$

and integrating once more, it is found that

$$\frac{0{\cdot}4 v_r}{U_f} = -\frac{y}{r}F(\zeta) - \frac{gy}{U_f^2}\frac{dh}{dr}\ln(1-\zeta) + \frac{Cy}{U_f^2}\ln\frac{\zeta}{1-\zeta} + C_1, \tag{9}$$

where $F(\zeta)$ denotes the function

$$F(\zeta) = \int_0^\zeta \frac{d\xi}{\xi(1-\xi)}\int_0^\xi f^2 d\xi.$$

The constants C and C_1 are determined by the following boundary conditions.

(i) According to Rozovskii (1961), the boundary condition at a rough wall is that

$$\tau_r/\tau_0 = v_r/v_\theta \tag{10}$$

should be valid for points near the wall. This condition is seen to be fulfilled when

$$C_1 = \frac{Cy}{U_f^2}\ln\frac{30y}{k_b}.$$

It may be noted that the same expression for C_1 is arrived at if we use the condition that v_r shall vanish at a distance $\frac{1}{30}k_b$ above the bed level, as was required for v_θ.

(ii) For a smooth wall, Rozovskii demonstrates that the condition is $\tau_r = 0$ close to the wall. Hence putting $\zeta = 1$ and $\tau_r = 0$ in (8) gives a relation for C:

$$C = \frac{U_f^2}{r}\int_0^1 f^2(\zeta)\,d\zeta - g\frac{dh}{dr}.$$

Finally, the last term in this expression is determined from the condition that the net flux through a vertical cross-section must vanish in the case of steady flow:

$$\int_0^1 v_r\,d\zeta = 0.$$

The calculated distributions of the tangential and radial velocity components are given in figure 2. The finite value of v_r at the upper wall is of course unrealistic. The true condition is that v_r decreases rapidly through the viscous sublayer and becomes zero at the wall.

Now it is possible to calculate the angle δ by which the shear-stress vector at

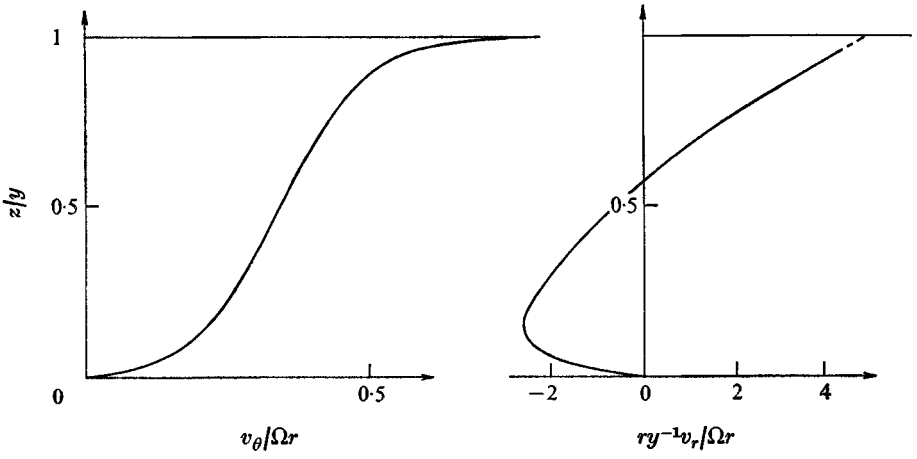

FIGURE 2. Distribution of tangential and radial velocity components.

the bed deviates from the mean flow direction. The value of δ is obtained from (10):

$$\tan\delta = \tau_r/\tau_\theta = v_r/v_\theta.$$

For the particular flow under consideration, (8) gives an expression of the form

$$\tan\delta = 21y/r, \tag{11}$$

where the coefficient, in principle, depends on the wall roughness. This dependence is very weak, however.

3. The basic flow

The next part of the problem is to determine the corresponding shape of the sand bed, assuming equilibrium and that the shear stress is sufficiently large to ensure sediment motion over the entire cross-section. In other words, the depth y used above varies with the distance r, and we are looking for the particular variation that will satisfy the continuity equation for the sediment, as derived below.

To this end, it is necessary first to consider the motion of bed particles in channels with a small transverse slope α; see figure 3. The direction of the shear stress is assumed to be nearly longitudinal and equal to the local flow direction close to the bed. Owing to the helicity it may, however, deviate from the direction of the mean flow by the angle δ, as explained above. Because of gravity, a migrating particle will tend to move downhill, hence following a path that deviates by some small angle from the flow direction. The problem is to determine the angle ψ between the particle path and the bed shear stress.

The balance of the longitudinal forces on a single sediment particle is described by the equation

$$F_D = (W - F_L)\cos\alpha\tan\phi,$$

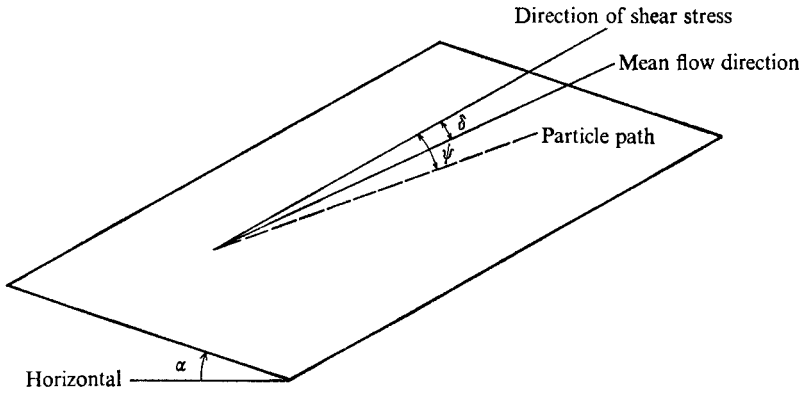

FIGURE 3. Particle moving on a plane with a transverse slope.

where F_D and F_L are the drag and lift forces on the particle, respectively, W is its submerged weight and ϕ is the dynamic friction angle. For small sediment transport rates, the velocity of the sediment particles is small compared with the flow velocity near the bed, as demonstrated by Luque (1974). Hence in this case the force on a particle will have a transverse component

$$(W - F_L)\sin\alpha - F_D \tan\psi.$$

As the mean acceleration of a particle is zero, this force component must be equal to zero, so that

$$\tan\psi = \tan\alpha/\tan\phi. \tag{12}$$

This relation is valid as long as the angle α is small compared with the angle of repose. In the following, it is assumed that (12) may be used to determine the direction of the sediment transport. It should be emphasized that this assumption becomes questionable if a large part of the sediment is carried in suspension. This restriction is, however, in agreement with the assumption of small sediment transport rates already applied.

Now (12) is applied to the steady and uniform flow in an annular flume with a movable bed. Because of the helical motion described above, there will be an inward component of sediment transport of magnitude $q_s \tan\delta$, where δ is determined from (11). However, in the case of steady flow, the net rate of radial sediment transport must be zero, as otherwise a stationary bottom cannot be attained. Hence, to counterbalance the inward radial transport due to the secondary flow, a radial bed slope must develop, giving increasing depths towards the outer side wall. Then the inward transport may be balanced by the outward component, which is due to the transverse slope of the channel bed. Equilibrium occurs for $\psi = \delta$, which according to (11) and (12) gives

$$\frac{\tau_t}{\tau_l} = \tan\delta = 21\frac{y}{r} = \frac{\tan\alpha}{\tan\phi},$$

or

$$\frac{1}{\tan\phi}\frac{dy}{dr} = 21\frac{y}{r}. \tag{13}$$

The solution of this equation is

$$y = cr^p, \quad \text{where} \quad p = 21\tan\phi \tag{14}$$

and c is a constant of integration. Equation (13) was found to describe the mean bottoms of all the experiments fairly well provided that p was taken equal to 8, which gives a dynamic friction angle $\phi = 21°$. For comparison, it may be mentioned that the angle of repose was measured to be 26°.

4. The perturbation equations

The uniform flow described above develops a bottom which is a surface of revolution given by (14). Experiments demonstrate that this basic flow is usually unstable, so that small perturbations will increase. To explain this, a stability analysis based on the equations for small perturbations must be carried out.

Because of the complicated nature of the problem, it seems reasonable to apply the simplest possible mathematical model that is likely to describe the essentials of the flow. Although the instability corresponds to an unsteady flow situation, it was found that the changes in the bed form are slow enough for the steady-state equations to be applied. Further, it has been assumed that the flow may be regarded as 'gradually varying', an approximation which has been found to be adequate in many similar cases, for instance meandering. This implies that only the mean values (over a vertical) of the velocity components, $\bar{v}_\theta$ and $\bar{v}_r$, occur in the momentum equation, and the correction factors are taken equal to unity. Under these assumptions, the momentum equation has the following two components:

$$\left.\begin{aligned} \bar{v}_r\frac{\partial\bar{v}_\theta}{\partial r} + \frac{\bar{v}_\theta}{r}\frac{\partial\bar{v}_\theta}{\partial\theta} + \frac{\bar{v}_\theta\bar{v}_r}{r} &= -\frac{1}{r}\frac{\partial}{\partial\theta}(gh) + \frac{\tau_{\theta t}-\tau_{\theta b}}{\rho y}, \\ \bar{v}_r\frac{\partial\bar{v}_r}{\partial r} + \frac{\bar{v}_\theta}{r}\frac{\partial\bar{v}_r}{\partial\theta} - \frac{\bar{v}_\theta^2}{r} &= -\frac{\partial}{\partial r}(gh) + \frac{\tau_{rt}-\tau_{rb}}{\rho y}. \end{aligned}\right\} \tag{15}$$

As before, the suffixes t and b refer to the top and bottom, respectively. In the second equation, the friction term is due to the helicity and is of moderate magnitude, so that its variations may be neglected. The friction term in (15) vanishes for uniform flow but may for non-uniform, gradually varying flow be estimated by the following calculation.

In the case of non-uniformity, the velocity distribution given by (6) should be modified to

$$v_\theta = 2{\cdot}5U_{fb}\ln\frac{30z}{k_b} - 2{\cdot}5U_{ft}\ln(1-\zeta),$$

where the suffixes b and t refer to the bottom and top boundaries, respectively. This modification is necessary to give the correct velocity distributions near

both boundaries and agrees well with results of Reid (1957). The velocity Ωr of the upper boundary then becomes

$$\Omega r = U_{fb} K_b + U_{ft} K_t, \tag{16}$$

in which

$$K_b = 2{\cdot}5 \ln (30y/k_b), \quad K_t = 2{\cdot}5 \ln (9U_{ft} y/\nu).$$

By integrating (15), the following important expression is obtained:

$$U_{fb} = (V - 2{\cdot}5U_{ft})/(K_b - 2{\cdot}5).$$

From this, U_{ft} may be eliminated by means of (16), so that we get an expression for the friction velocity along the bed in terms of the mean velocity V:

$$U_{fb} = (V - 2{\cdot}5\Omega r/K_t)\,[K_b - 2{\cdot}5(1 + K_b/K_t)]^{-1},$$

which will be applied in the following. In the same way, we may derive an expression for U_{ft}:

$$U_{ft} = \frac{1}{K_t}\left[\Omega r - \left(V - \frac{2{\cdot}5\Omega r}{K_t}\right)\left\{1 + \frac{2{\cdot}5(1 + K_b/K_t)}{K_b - 2{\cdot}5(1 + K_b/K_t)}\right\}\right].$$

To establish the momentum equation, it is necessary to calculate the difference

$$(\tau_{\theta t} - \tau_{\theta b})/\rho = U_{ft}^2 - U_{fb}^2$$

between the boundary shear stresses by using the expressions derived above. Assuming small deviations from the basic flow we find

$$U_{ft}^2 - U_{fb}^2 = -\beta U_f^2 u,$$

where u is the relative deviation of the true mean velocity from that of the basic flow [see (20)] while

$$\beta = 2\left[\left(\frac{K_b}{K_t}\right)^2 + \frac{K_b}{K_t}\right] \Big/ \left[\frac{K_b}{K_t} - \frac{2{\cdot}5}{K_t}\left(1 + \frac{K_b}{K_t}\right)\right].$$

The equation of continuity reads

$$\frac{\partial}{\partial r}(r\bar{v}_r y) + \frac{\partial}{\partial \theta}(\bar{v}_\theta y) = 0. \tag{17}$$

Finally, if the sediment transport mainly occurs as bed load, the sediment continuity equation is

$$\frac{1}{r}\frac{\partial}{\partial r}(r q_{sr}) + \frac{1}{r}\frac{\partial q_s}{\partial \theta} = (1 - e)\frac{\partial y}{\partial t}, \tag{18}$$

in which q_s is the circumferential transport rate (volume of sediment substance per second per unit width), q_{sr} is its radial component, e is the porosity and t is the time.

The next step in the analysis is the linearization of the equations. It is assumed that the original bed is given a small periodic perturbation, which will also change the originally uniform velocity field. The following substitutions are introduced:

$$y = y_0(1 + \eta), \quad gh = g(h_0 + \Phi), \tag{19}$$

a suffix zero indicating the unperturbed quantity. For the velocity components we write

$$\bar{v}_\theta = V(1+u), \quad \bar{v}_r = vV. \tag{20}$$

The quantities η, u and v are non-dimensional and supposed to be so small that second and higher powers may be neglected. V is the mean velocity of the basic flow and consequently proportional to Ωr:

$$V = \alpha \Omega r, \tag{21}$$

where α is a factor between 0 and 1. Substitution of (19) and (20) into the flow equations and subsequent linearization gives the following result:

$$\frac{V^2}{gr}\left[\frac{\partial v}{\partial \theta} - 2u\right] = -\frac{\partial \Phi}{\partial r}, \tag{22a}$$

$$\frac{V^2}{gr}\left[v\left(1+\frac{r}{V}\frac{dV}{dr}\right)+\frac{\partial u}{\partial \theta}\right] = -\frac{1}{r}\frac{\partial \Phi}{\partial \theta} - \frac{\beta U_f^2 u}{g y_0}, \tag{22b}$$

$$\frac{v}{r}\left[1+\frac{r}{V y_0}\frac{d}{dr}(V y_0)\right] + \frac{\partial v}{\partial r} + \frac{1}{r}\frac{\partial u}{\partial \theta} = -\frac{1}{r}\frac{\partial \eta}{\partial \theta}. \tag{22c}$$

By use of (14) and (21) the last two equations may be rewritten as

$$\frac{V^2}{gr}\left[2v + \frac{\partial u}{\partial \theta}\right] = -\frac{1}{r}\frac{\partial \Phi}{\partial \theta} - \frac{\beta U_f^2}{g y_0} u, \tag{23}$$

$$(p+2)\frac{v}{r} + \frac{\partial v}{\partial r} + \frac{1}{r}\frac{\partial u}{\partial \theta} = -\frac{1}{r}\frac{\partial \eta}{\partial \theta}. \tag{24}$$

The periodicity of the small perturbation is now introduced by making the assumption that

$$\eta = \eta_0(r)\exp\left[in(\theta - \omega t)\right], \tag{25a}$$

$$u = u_0(r)\exp\left[in(\theta - \omega t)\right], \tag{25b}$$

$$v = v_0(r)\exp\left[in(\theta - \omega t)\right], \tag{25c}$$

where ω is the angular speed of the perturbation and the integer n is the number of periods. Substitution of these expressions into the flow equations and elimination of Φ by cross-differentiation give the following relation between u_0 and v_0:

$$u_0[4+(p-3)\kappa] + r u_0'(1-\kappa) = i v_0\left(n + \frac{4}{n}\right) + \frac{2i}{n} r v_0', \tag{26}$$

where a prime denotes differentiation with respect to r and κ is an abbreviation for the quantity

$$\kappa = \frac{i}{n}\beta\left(\frac{U_f}{V}\right)^2 \frac{r}{y_0}.$$

Similarly, we get from the continuity equation the relation

$$u_0 = -\eta_0 + (i/n)\left[(p+2)v_0 + r v_0'\right], \tag{27}$$

which may be used to eliminate u_0 from (26). This results in the equation

$$\frac{ia}{n}r^2v_0''+rv_0'[(p+3)a+b-2]\frac{i}{n}+v_0\frac{i}{n}[(p+2)b-n^2-4]=b\eta_0+ar\eta_0', \quad (28)$$

in which $a=1-\kappa$ and $b=4+(p-3)\kappa$.

Next we turn to the sediment equation (18), where the linearization is a little more complicated. The local value of q_s is assumed to vary as the local mean velocity to some power m, i.e.

$$q_s \sim V^m(1+mu) \sim r^m(1+mu). \quad (29)$$

According to the previous arguments, the direction of the mean velocity forms the angle δ with the bed shear stress and the angle ψ with the direction of the sediment transport. Consequently, the radial component of the sediment transport rate is

$$q_{sr}=q_s[v+\tan(\psi-\delta)].$$

Assuming that ψ and δ are small, the substitution of (11) and (12) gives

$$q_{sr}=q_s\left[v+\frac{1}{\tan\phi}\frac{\partial y}{\partial r}-21\frac{y}{r}\right].$$

If, next, $y=y_0(1+\eta)$ is inferred and linearization is carried out, the expression for the radial sediment transport rate becomes

$$q_{sr}=q_s\left[v+\frac{y_0}{\tan\phi}\frac{\partial\eta}{\partial r}\right]+q_s(1+\eta)\left[\frac{1}{\tan\phi}\frac{dy_0}{dr}-21\frac{y_0}{r}\right],$$

where the last term disappears because of (13), which is valid for the basic flow. The resulting expression is then

$$q_{sr}=q_s\left[v+\frac{y_0}{\tan\phi}\frac{\partial\eta}{\partial r}\right]. \quad (30)$$

The boundary condition along the two side walls is that the radial component of the sediment transport must vanish. As the radial velocity v is also zero here, this boundary condition may be expressed as

$$\partial\eta/\partial r=0. \quad (31)$$

When (29) and (30) are inserted in the total transport equation (18), the following basic equation is obtained:

$$imnu_0+(m+1)\left[v_0+\frac{y_0}{\tan\phi}\eta_0'\right]+r\frac{\partial}{\partial r}\left[v_0+\frac{y_0}{\tan\phi}\eta_0'\right]=-\frac{ry_0}{q_s}(1-e)in\omega\eta_0,$$

from which u_0 may be eliminated by means of (27). This gives

$$(1-m-mp)v_0-(m-1)rv_0'+(m+1)\frac{y_0}{\tan\phi}\eta_0'+r\frac{d}{dr}\left(\frac{y_0}{\tan\phi}\eta_0'\right)$$
$$=in\eta_0[m-\omega(1-e)ry_0/q_s]. \quad (32)$$

5. Solution of the equations

As the equations are too complicated to allow an exact analytical solution, it is necessary to develop a numerical procedure based on the values of the physical parameters prevailing in the experiments. From preliminary test series it was found that the dynamic friction angle of the bed material was consistently about 21°, so that it is possible to evaluate one of the most important parameters:

$$p = 21 \tan \phi \simeq 8.$$

The exponent m in the transport relation (29) is extremely difficult to measure. At large transport rates m is about 3 (cf. Meyer-Peter & Müller's (1948) bed-load equation) while its value is extremely large for small transport rates close to the threshold of particle motion. As the present investigation is concerned with small transport rates, it was decided to take $m = 6$. The principal results are not sensitive to this choice.

An estimate of the wall roughness led to the values $K_b = 11{\cdot}5$ and $K_t = 20$, but it is, of course, an approximation to apply constant values over the entire channel bed.

The equations were solved by successive approximations, starting with the assumed relation

$$\eta_0 = a_0 + af(r/b), \tag{33}$$

where f is a real function, b is the channel width, while a is a complex quantity. Without losing generality a_0 may be put equal to unity. A graph of f is given in figure 4. Note that the condition $\eta_0' = 0$ at the side wall is satisfied.

When the above specific numerical values of the flow parameters are adopted, (28) can be replaced by two simultaneous equations, on separating real and imaginary contributions by putting $v_0 = v_r + iv_i$:

$$\left.\begin{aligned} L(v_r) &= i\kappa M(v_i) - i\kappa[5\eta_0 + r\eta_0'], \\ L(v_i) &= -(4\eta_0 + r\eta_0') - i\kappa M(v_r), \end{aligned}\right\} \tag{34}$$

in which the operators L and M are defined by

$$\left.\begin{aligned} L(v_0) &= r^2 \frac{d^2 v_0}{dr^2} + 13r \frac{dv_0}{dr} + (36 - n^2) v_0, \\ M(v_0) &= r^2 \frac{d^2 v_0}{dr^2} + 6r \frac{dv_0}{dr} - 50 v_0. \end{aligned}\right\} \tag{35}$$

By substitution of some estimated variations of the right-hand sides of (34) and subsequent integration, improved variations are obtained. After each iteration, the arbitrary constants are determined from the boundary condition that v_0 must vanish at the side walls. As κ is usually a rather small quantity, the first estimate of v_0 may be obtained by putting $\kappa = 0$, which permits immediate integration of (34). Although κ is small, it is of great importance for the stability, as $\kappa = 0$ leads to stability for all the modes investigated. In the actual calculations, it is appropriate to separate both v_r and v_i into two parts, corresponding to the two terms in (33).

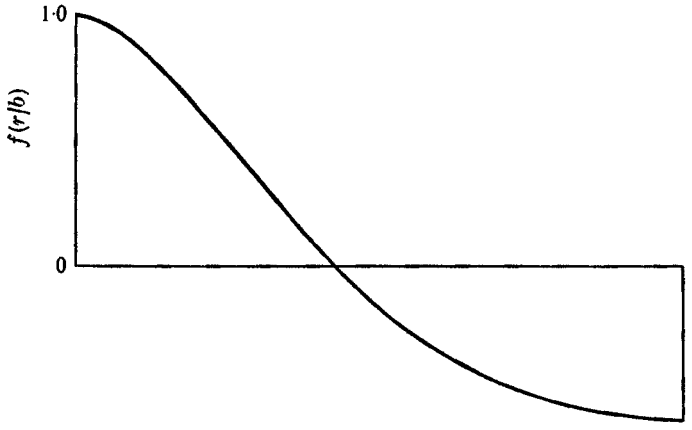

FIGURE 4. The function f from (33).

The next step in the analysis concerns (32), which under the same conditions as above can be rewritten in the form

$$\frac{1}{r^6}\frac{d}{dr}\left[\frac{y_0 r^7}{\tan\phi}\eta_0'\right] = in[6 - d\omega r^3]\,\eta_0 + 53v_0 + 5rv_0'; \tag{36}$$

$$d = (1-e)\,D/q_{s0}r_0^2,$$

where D and q_{s0} are the depth and sediment transport rate at the reference distance r_0. The previously obtained expression for v_0 and (33) are inserted into the right-hand side of this equation. Integration can now be carried out directly, and the resulting variation of η_0 compared with the assumed variation. The eigenvalue $\beta\omega$ is determined by the boundary condition that η_0' should vanish at the side walls.

ω is assumed to be complex, so that $\omega = \omega_r + i\omega_i$. The sign of ω_i determines the stability condition, positive values indicating instability. As long as the perturbations are small, they are known to grow exponentially, the degree of amplification being determined by the quantity $n\omega_i$. Hence, of all possible unstable modes, the one corresponding to the largest value of the amplification coefficient $n\omega_i$ will rapidly become dominant.

6. Comparison with experiments

A sketch of the experimental set-up is given in figure 5. The annular flume has an outer diameter of 2 m and a width of 20 cm. It is covered with an annular plate, which can be made to rotate by the electromotor indicated to the left of the figure. When the sediment is introduced into the flume and its surface has been given the desired shape, water is carefully supplied and the plate brought in contact. After each experiment, the cover is removed and the water is let out, in some case stepwise, so that the bed-elevation contours become visible (cf. figure 6, plate 1). When all the water has been removed, the bed surface can be conveniently surveyed by means of a point gauge.

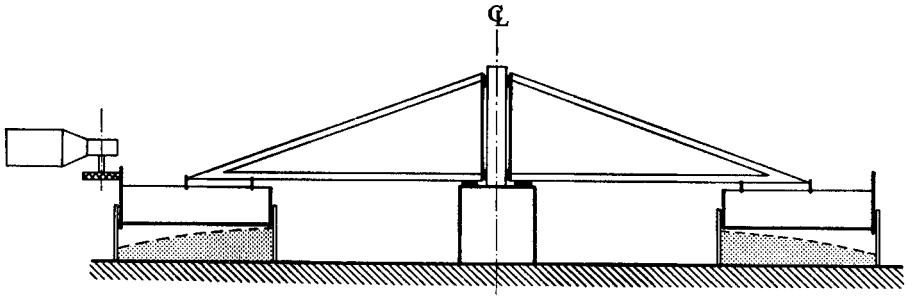

FIGURE 5. Cross-section of experimental set-up.

An interesting consequence of the previous analysis is that, according to (14), the sediment bed is a surface of revolution, depending on the degree of filling (characterized for instance by the maximum depth D) and on the dynamic friction angle ϕ. A necessary condition for this description to be adequate is, of course, that ϕ be at least approximately independent of the flow conditions.

The question of the applicability of (14) has been tested by additional experiments using two different sand types with grain diameters of 0·25 and 0·75 mm. Some typical results are presented in figures 7 (*a*) and (*b*).

One difficulty is that in most cases the original sand bed is unstable and that the formation of sand waves may affect the particle motion and hence the value of the dynamic friction angle. However, it is still possible that the mean bed, after averaging of the depth over several periods, may be described by (14), and this was actually found to be the case, at least to a first approximation. The corresponding value of ϕ exhibited some variation but was for moderate transport rates found to be about 25°.

The form of the mean bed was found to be nearly independent of the speed of rotation as long as the particles moved mainly as bed load. Figure 7 (*a*) gives an example where the tractive shear was increased by a factor of 5 without causing an appreciable change in the transverse slope. When, on the other hand, the rotation became so rapid that the particles moved mainly in suspension, the bed form changed rather drastically and the bed waves disappeared or were at least appreciably reduced. As (14) was derived under the assumption of negligible suspension, this result is not surprising.

It may be relevant to remark that previous investigations of flow in open channel bends (Engelund 1974) indicated a value of about $\phi = 27°$. The agreement with the present result is significant because the strength of the helicity in an open channel is only a fraction of that in Couette flow.

The conclusion of this investigation is that (14) seems to be applicable at moderate transport rates, implying a dynamic angle somewhat smaller than the angle of repose. This was also found to be consistent with the artificially low density of the sediment used in the main experiment, where the purpose was to investigate the growth of the sand waves.

In these experiments, the surface of the sediment was given a shape corresponding to (14) before the cover was rotated. As explained above, the instability gave rise to very regular and sinusoidal disturbances of increasing amplitude.

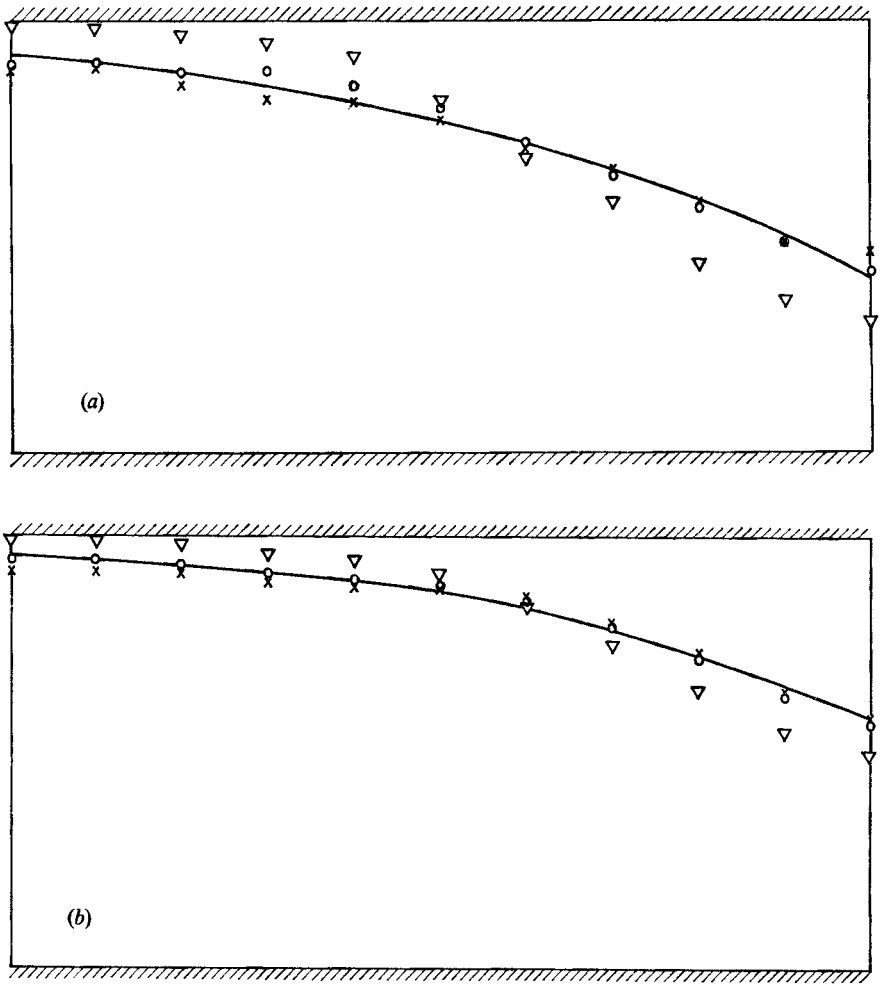

FIGURE 7. Mean bed elevation for different speeds of rotation. (*a*) Grain diameter = 0·25 mm; ×, $\omega = 1{\cdot}3\ \mathrm{s}^{-1}$; ○, $\omega = 2{\cdot}9\ \mathrm{s}^{-1}$; ▽, $\omega = 3{\cdot}7\ \mathrm{s}^{-1}$. (*b*) Grain diameter = 0·75 mm; ×, $\omega = 1{\cdot}9\ \mathrm{s}^{-1}$; ○, $\omega = 2{\cdot}4\ \mathrm{s}^{-1}$; ▽, $\omega = 3{\cdot}0\ \mathrm{s}^{-1}$. The curve corresponds to (14) with $\phi = 26°$.

The coarse low-density material was chosen because the large grain size prevented the formation of the small surface ripples observed when fine sand is applied. These ripples, also produced by flow in straight flumes, have nothing to do with the present instability problem.

Experiments were run with two different maximum depths: $D = 4$ and 6 cm. In the case of smaller depth, the number of periods n was consistently found to be seven as long as the height of the sand waves was small and the undulations regular. When the experiment was continued beyond this initial state, the waves became irregular and their number decreased to six or five. In the case of larger depth, the initial instability was found to yield six periods, which in the mature stage were occasionally reduced to five.

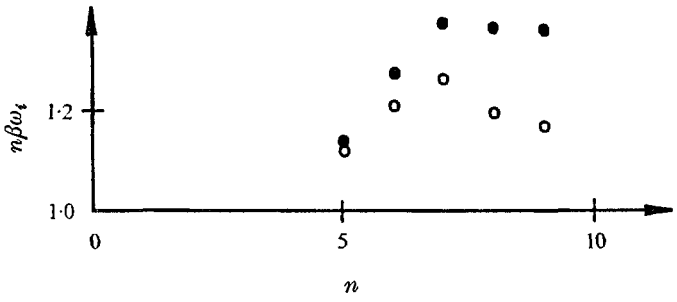

FIGURE 8. Amplification coefficient *vs.* n. ●, D = 4 cm; ○, D = 6 cm.

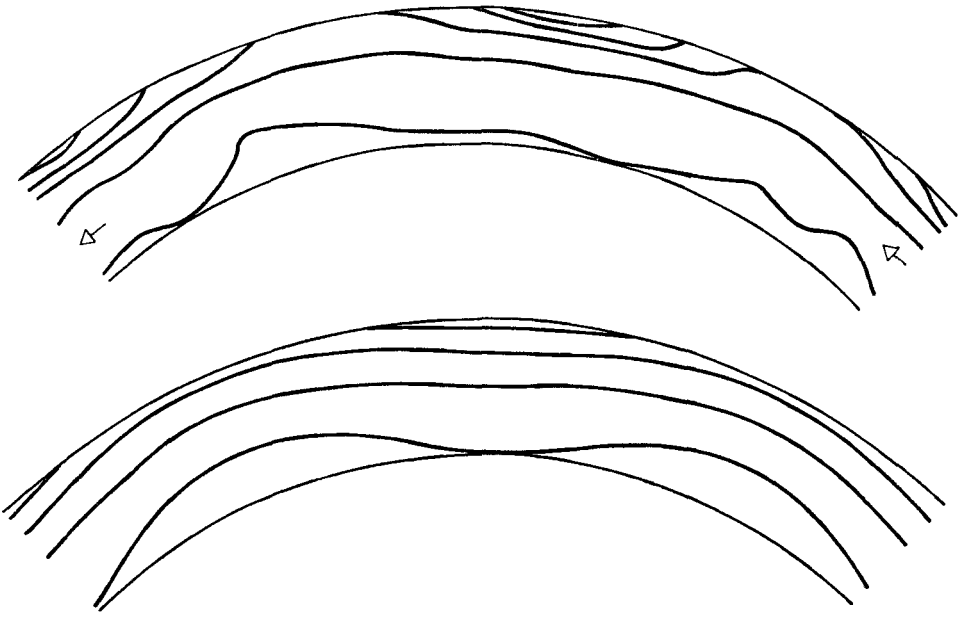

FIGURE 9. Comparison between measured (above) and calculated bed-elevation contours. The maximum mean depth is 3·8 cm; the number of periods is n = 7. Contour interval = 1 cm.

These observations can now be compared with the results of the stability analysis, as given in figure 8, where the amplification coefficient is plotted against the number of periods. As mentioned previously, a positive value of ω_i indicates that the modes considered are in fact unstable. The calculations were carried out for the same two depths as in the experiments, and in both cases the maximum value occurred for n = 7. For the smaller depth, this agrees with the observations, but for the large depth, the observed number is six.

It is not clear whether this discrepancy is due to inaccuracies in the basic assumptions underlying the theory, incorrect estimates of the parameters or simply to the fact that the influence of the outer side wall must necessarily increase with increasing depth. This influence has been neglected in the analysis, which assumes the depth to be small compared with the channel width.

As a further test, the calculated eigenfunction has been used to predict the shape of the bed waves for the most unstable mode. Figure 9 gives a comparison between the measured and calculated bed-elevation contours.

The author is indebted to Leif Tegneby for his careful design and execution of the necessary experimental equipment and for valuable assistance during the measurements.

REFERENCES

ENGELUND, F. 1974 Flow and bed topography in channel bends. *Proc. A.S.C.E.* **100** (HY11), 1631–1648.

GRAF, W. 1971 *Hydraulics of Sediment Transport.* McGraw-Hill.

HOOKE, R. L. 1974 Shear-stress and sediment distribution in a meander bend. *University of Uppsala, Sweden, Ungi Rep.* no. 30.

LARRAS, J. 1972 Hydraulique et granulats. *Collection du Centre de Recherches et d'Essais de Chatou.*

LUQUE, R. F. 1974 Erosion and transport of bed sediment. Dissertation, Krips Repro B. V.-Meppel.

MEYER-PETER, E. & MÜLLER, R. 1948 Formulas for bed-load transport. *Proc. 3rd Meeting, Int. Ass. Hydr. Res., Stockholm.*

RAUDKIVI, A. J. 1967 *Loose Boundary Hydraulics.* Pergamon.

REICHARDT, H. 1959 Gesetzmässigkeiten der geradlinigen turbulenten Couetteströmung. *Rep. Max-Planck-Inst.* für Strömungsforschung *aerodynamischen Versuchsanstalt. Göttingen*, no. 22, pp. 1–45.

REID, R. O. 1957 Modification of the quadratic bottom-stress law for turbulent channel flow in the presence of surface wind-stress. *Beach Erosion Board, Corps. Engrs, Tech. Memo.* no. 93.

ROZOVSKII, I. L. 1961 Flow of water in bends of open channels. *Israel Program for Scientific Translations, Jerusalem.*

ZIMMERMANN, C. 1974 Einfluss der Sekundärströmung auf den Faststoftransport in Gerinnen. Dissertation, University of Karlsruhe, Germany.

ZIMMERMANN, C. & KENNEDY, J. F. 1973 Sediment transport and bed forms in laboratory streams of circular plan form. *Proc. I.A.H.R.* **1**, 1–8.

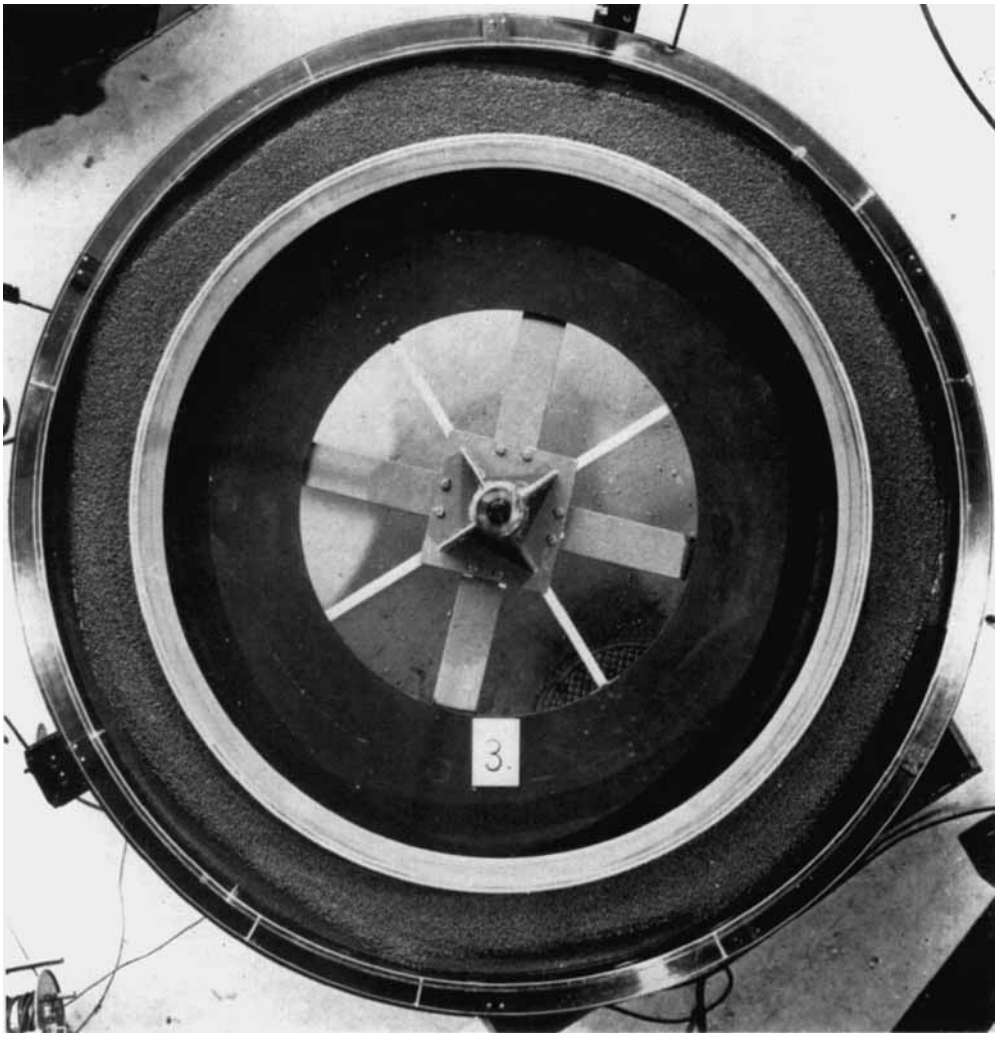

FIGURE 6. Photograph taken after removal of the cover and partial draining of the channel.